Available online at www.sciencedirect.com
SCIENCE DIRECT
Catalysis Today 105 (2005) 106–121
CATALYSIS TODAY
www.elsevier.com/locate/cattod

The roles of gallium hydride and Brønsted acidity in light alkane dehydrogenation mechanisms using Ga-exchanged HZSM-5 catalysts: A DFT pathway analysis

Yogesh V. Joshi, Kendall T. Thomson *

School of Chemical Engineering, Purdue University, West Lafayette, IN 47907, USA

Abstract

We have used density functional theory (DFT) to study light alkane dehydrogenation by Ga-exchanged HZSM-5 by considering two types of catalytic sites: a mono-Al site of the form $Z^-[HGaX]^+$ (X = H, CH_3, OH, Cl) and a di-Al site of the form $Z^{2-}[GaH]^{2+}$. For the mono-Al site, we report a new, direct one-step dehydrogenation mechanism; however, we conclude in general that mono-Al sites in ZSM-5 are not likely responsible for alkane dehydrogentation, as calculated activation energies are too high compared to experimental values (~60 kcal/mol versus 39 kcal/mol). Instead, we propose $[GaH]^{2+}$ residing near di-Al sites ($Z^{2-}[GaH]^{2+}$) are more active sites for dehydrogenation. We report a three-step mechanism for di-Al sites consisting of (1) C–H activation, followed by (2) alkene desorption and (3) H_2 removal. We find that as Al–Al distance increases, the activation barrier for C–H activation decreases (ranging from 85.72 to 38.38 to 19.69 kcal/mol), while the barrier for H_2 removal increases (ranging from 15.49 to 36.71 to 47.38 kcal/mol)—resulting in an optimal Al–Al separation distance of 4.53 Å arising from these competing trends. As a result, we propose a simple 'structure-to-activity' correlation based on the Sabatier principle, which could be used to model and design the catalyst with required dehydrogenation activity.

Keywords: Ga-HZSM-5; Density functional theory; Dehydrogenation; Light alkane aromatization; Bifunctional mechanism; Sabatier principle

1. Introduction

Light alkane aromatization using shape selective MFI-based catalysts is an important chemical process to upgrade light alkane feedstocks like liquefied petroleum gas (LPG). The valuable aromatics produced by this process find important commercial applications in downstream processes. Unfortunately, the substantial cracking activity of unmodified HZSM-5 catalyst leads to a large selectivity for C1 and C2 products. This problem is overcome by adding additional dehydrogenation function in the form of extra-framework species like Ga, Zn and Pt. The improved activity and selectivity due to these extra-framework species has made possible commercial applications such as the Cyclar and Aeroforming processes. The elevated hydrogenolysis activity of Pt-based catalysts and the volatility of Zn species in H_2 at higher temperatures, has lead to the identification of Ga-HZSM-5 catalysts as a commercially viable choice [1]. See the recent review by Fricke et al. [2] covering various applications of Ga-based zeolite catalysts.

There has been a constant effort to improve the selectivity of these catalytic systems by understanding the role of the extra-framework species. A large number of experimental investigations of gallium oxides and Ga-HZSM-5 catalysts have been reported [3–23] in the literature. Some review articles [24–26] provide a concise summary of all the experimental work done in the past. For a pure Brønsted acid catalyzed mechanism, hydride transfer has been identified as an important reaction path for initial removal of hydrogen from light alkanes. However, this redistribution of the hydrogen in the lower alkanes causes reduction in the aromatics selectivity. A study involving careful comparison of the initial cracking rates versus dehydrogenation rates

* Corresponding author. Tel.: +1 765 496 6706; fax: +1 765 494 0805.
E-mail address: thomsonk@purdue.edu (K.T. Thomson).

0920-5861/$ – see front matter © 2005 Published by Elsevier B.V.
doi:10.1016/j.cattod.2005.04.017

[27] for HZSM-5 concluded that the same Brønsted acid site is involved in the dehydrogenation as in cracking. Thus, to enhance dehydrogenation in comparison with cracking one needs to change the initial dehydrogenation mechanism completely. Hence, the additional dehydrogenation function by extra-framework Ga improves selectivity with simultaneous generation of molecular hydrogen as a valuable side product. Also, experimentally it has been observed [11,28] that propene is far more reactive than propane, and hence it was concluded that initial dehydrogenation is likely to be the rate-limiting step.

Initially, it was suggested that the gallium oxide phase was the source of the catalytic activity in Ga-HZSM-5, as it was shown that Ga_2O_3 is capable of H_2 dissociation [7], dehydrogenation and dehydrocyclization [6,12]. However, it was found that the intrinsic dehydrogenation activity of Ga_2O_3-HZSM-5 is better than that of Ga_2O_3 alone. The decrease in the dehydrogenation activity of Ga_2O_3-HZSM-5 upon exchange of Brønsted protons with Na^+ lead to the conclusion that this catalyst operates via a bifunctional mechanism [4]. In the proposed mechanism by Meriaudeau and Naccache [4], the Ga–O coordination from oxide phase activates the C–H bond and the alkoxide species is exchanged with a Brønsted acid site. Eventually, both H_2 and the alkene desorb to regenerate the active sites. There are several other studies [15,29,30] proposing bifunctional mechanisms; however, they differ with respect to the details of the mechanistic steps. Iglesia et al. [29] concluded that Brønsted acid sites cause C–H activation, while Ga is responsible for recombinative desorption of the surface hydrogen atoms. Gnep et al. [30] proposed that Ga sites and Brønsted sites work independently, where Ga carries out dehydrogenation, while regular Brønsted acid sites catalyze oligomerization, β-scission and cyclization steps. This hypothesis was further supported by the work from Kwak and Sachtler's group [16], where they located an optimum [Ga]/([Ga] + [H^+]) ratio for activity and selectivity in Ga-HZSM-5. A hydrogen back-spillover phenomenon [31] has been proposed to support the H_2 removal ability of Ga species from the distant Brønsted sites.

Some experimental efforts were also aimed at elucidating the nature of the active site. By studying the extent of reduction of Ga–H/Na-ZSM-5, Price and Kanazirev [23] concluded that the active catalyst consists of Ga in its reduced state. They concluded that Brønsted acid sites play an important role in the reduction of gallium oxide species. Using in situ Ga K-edge X-ray adsorption spectroscopy, Meitzner et al. [32] showed that for the catalysts under working conditions, the nature of the active Ga species is GaH_x. This was further confirmed by recent work from Kazansky et al. [33] using DRIFTS. The authors showed that the characteristic Ga–H bond stretching frequency indicates the heterogeneity of GaH_x species on the catalyst surface. Also, CO adsorption studies pointed out the presence of the three types of sites in the reduced catalyst: (a) $[HGaH]^+$, (b) $[HGaOH]^+$ and (c) low coordinated Ga^+. The authors pointed out that the relative populations of these sites were very sensitive to the H_2 partial pressure and temperature. The Ga–H stretching band showed decreased intensity after evacuation at the higher temperature. However, it is not clear, which one is the active site for dehydrogenation.

Compared to the experimental literature, theoretical investigations of the dehydrogenation mechanism, and the nature of the active site for this system, are limited. Methane activation on $[Ga{=}O]^+$ species was studied by Himei et al. [34] and Broclawik et al. [35]. Gonzales et al. [36] studied the reduction process of $[Ga(OH)_2]^+$ by considering interconversion of different gallium species such as $[Ga{=}O]^+$, $[HGaOH]^+$, Ga^+ and $[HGaH]^+$. Their study concluded that $[HGaOH]^+$ species are kinetically the most favored species. However, this study could not explain the experimentally observed higher activity of the Ga-HZSM-5 for H_2/D_2 exchange. Frash and van Santen [37] considered a similar gallium site to study the ethane dehydrogenation reaction pathway. The authors classified the reaction paths as of two types: (i) a 'carbenium activation' pathway consisting an alkoxide-like intermediate along the reaction path after the activation of the C–H ($R^{\delta+}$–$H^{\delta-}$) bond and (ii) an 'alkyl activation' pathway supporting the formation of Ga–C coordination after the activation of the C–H bond ($R^{\delta-}$–$H^{\delta+}$). After a detailed analysis the authors concluded that the alkyl activation path for $[HGaH]^+$ species is the actual path for dehydrogenation. However, this conclusion was based on the observation that at higher temperatures, the initial C–H activation step becomes the rate-determining step, and the calculated activation barrier (39–40 kcal/mol) for this first step is in close agreement with the experimentally estimated value of 39 kcal/mol [20]. These trends in the reaction rate and change in the rate-determining step at higher temperature were mainly contributed by the entropy loss during the formation of the surface activated complex. With explicit consideration of physisorbed species under the influence of van der Waal's interactions, it will be difficult to draw similar conclusions. The entropy loss from a gas phase reactant to an active intermediate cannot be entirely assigned to the initial step of the reaction mechanism, as the motion of the molecule is already confined to the zeolite channel system. However, to study initial adsorption process quantitatively, a QM/MM model of the active site [38] is needed as it explicitly accounts for the van der Waal's attractive interactions. In general, we can say there are disagreements between the experimental results and the calculations. Hence, further investigations are necessary to confirm the nature of the active sites and other possible dehydrogenation mechanisms.

In this contribution, we used electronic density functional theory (DFT) to study dehydrogenation mechanisms catalyzed by Ga-exchanged HZSM-5. For the active sites like $Z^-[HGaX]^+$ (X=H, CH_3, OH, Cl), we first proposed a direct dehydrogenation (one-step) mechanism for light alkane dehydrogenation. These extra-framework species can possibly exist as an active site under reaction conditions and

provide an opportunity to study the effect of polar environment on one-step dehydrogenation mechanisms. These sites consist of gallium species next to one framework aluminum. There have been significant disagreements [39,40] in the literature regarding the distribution of Al in the zeolite framework. It has been shown [41] that pairs of framework Al provide a significant polar environment. Hence, we have also considered the possibility of Ga species near two-framework Al for our investigations. In doing so, we have concentrated on the effect of the Al–Al distance on the energetics of the 'carbenium activation' reaction path. The rest of this paper is organized as follows. In Section 2, we describe the details of the computational method and cluster selection. Section 3 consists of the results and discussions. In this section, we report the direct dehydrogenation path on $Z^-[HGaX]^+$ and the carbon number dependence of the activation barrier. In the same section, we put fort the reaction path for $Z^{2-}[GaH]^{2+}$ catalytic site (dual Al-sites). In Section 4, we summarize the conclusions of our work.

2. Cluster models and computational details

The ZSM-5 pore structure (MFI) consists of straight channels and sinusoidal channels running perpendicular to each other. The most active sites are generally thought to be located at the cross-section of these channels, as they are easily accessible by the reactants. In this work, we employed a cluster approximation to model the active sites in Ga-ZSM-5. All the clusters we used employed Si-H terminations with fixed bond lengths of 1.4979 Å (the computed bond distance for free SiH_4 using the equivalent level of the theory). The terminal Si and H atoms were then held fixed at their initial Cartesian positions for all subsequent calculations. The clusters were selected to represent two types of active sites; sites consisting of one framework aluminum and sites consisting of two-framework Al atoms. For the first type of site, our cluster consisted of 11 T sites from the ZSM-5 lattice structure as reported in the literature [42]. These lattice positions were located around the T12 position at the cross-section of the straight channel and the sinusoidal

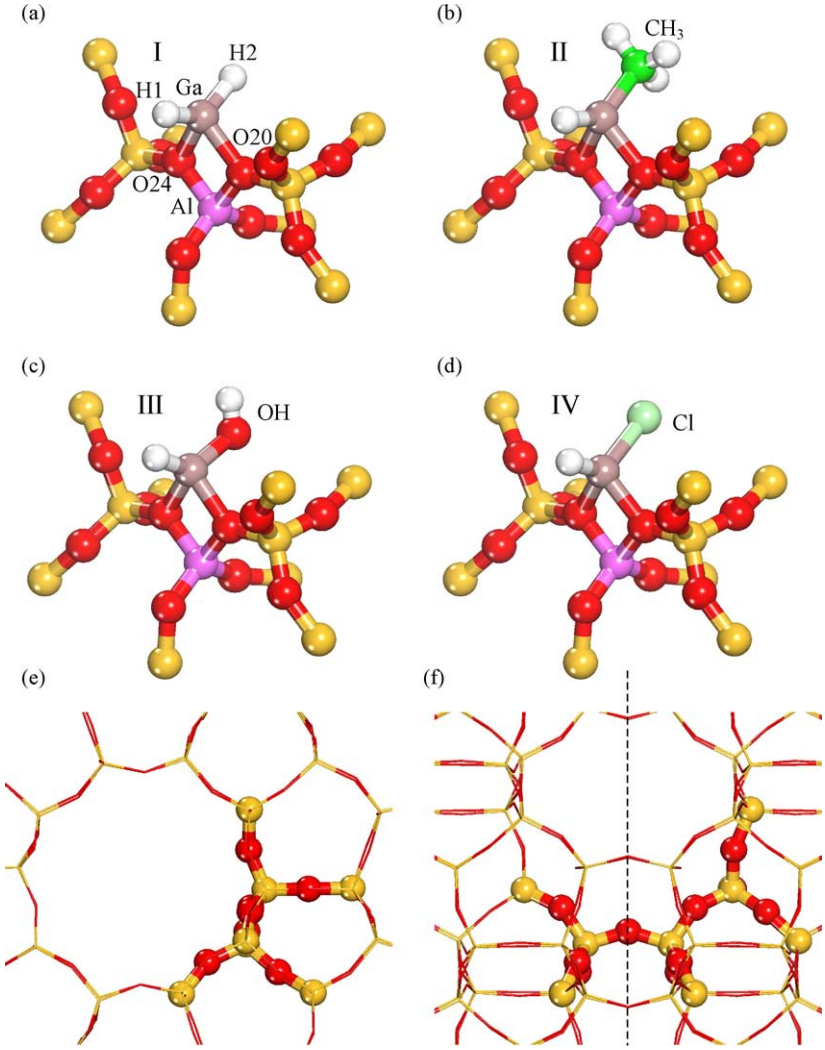

Fig. 1. Four different forms of the $Z^-[HGaX]^+$ species (I, II, III, IV): (a) X = H, (b) X = CH_3, (c) X = OH and (d) X = Cl. Location of the cluster in the MFI framework: (e) view along the straight channel and (f) view along the sinusoidal channel showing plane of symmetry.

channel. It has been shown that this size of the cluster is sufficiently accurate for the system under consideration, as Gonzales et al. [36] showed near-convergence of the various heats of reactions for a five T cluster. Si^{4+} at the T12 position was replaced by Al^{3+} and charge-compensated by an extra-framework cationic species. In our investigation, we considered the effect of different extra-framework gallium species on the one-step reaction pathway for dehydrogenation. The geometries of these clusters (I–IV) are shown in Fig. 1. The location of the 11 T cluster in the MFI framework is shown in Fig. 1e and f. The Mulliken charge on the Ga atom increases as the electronegativity of the bonded atom increases as listed in Table 1.

Table 1
Comparison of the geometry and charge parameters for four $Z^-[HGaX]^+$ species: X = H (I), CH_3 (II), OH (III) and Cl(IV)

	I	II	III	IV
Ga–X (Å)	1.566	1.967	1.817	2.180
Ga–H1 (Å)	1.557	1.554	1.548	1.542
Ga–O24 (Å)	1.967	1.983	1.955	1.939
Ga–O20 (Å)	2.001	2.011	1.964	1.965
Charge on Ga	0.419	0.523	0.641	0.553
EN[a]	2.20	2.55	3.44	3.16
ΔH_0 (kcal/mol)[b]	0.00	−3.334	18.792	27.853

[a] Pauling electronegativity.
[b] Heat of reduction for reaction $Z^-[HGaX]^+ + H_2 \Leftrightarrow Z^-[HGaH]^+ + HX$ at 298.15 K and 1 atm.

Our second type of active site model consisted of a gallium species $[GaH]^{2+}$ next to two aluminum sites. We considered three different clusters for this type of site. The first cluster (V) was a six-membered ring located along the straight channel and consisted of two T11, two T12 and two T07 tetrahedral T sites. In total, the cluster model contained 10 T sites. The location of the 10 T cluster in the MFI framework is shown in Fig. 2d. The silicon atoms at the two T11 positions were replaced by Al atom. A charge compensating $[Ga–H]^{2+}$ was symmetrically placed between the two Al atoms, coordinated with four proximal oxygens from the ring with an observed Ga–O distance of 2.02 Å. For the optimized geometry, the distance between two Al atoms was 4.53 Å. In order to study the effect of ring size on the dehydrogenation reaction, we considered a second type of $Z^{2-}[GaH]^{2+}$ models (VI and VII) consisting of an elongated eight-membered ring. In total, this cluster consists of 14 T sites. The location of this cluster, representing an eight-membered ring, is shown in Fig. 2e. The bare silicalite structure has a plane of symmetry as shown in Fig. 2d or e. This gives rise to pairs of T12 and T07 positions in the

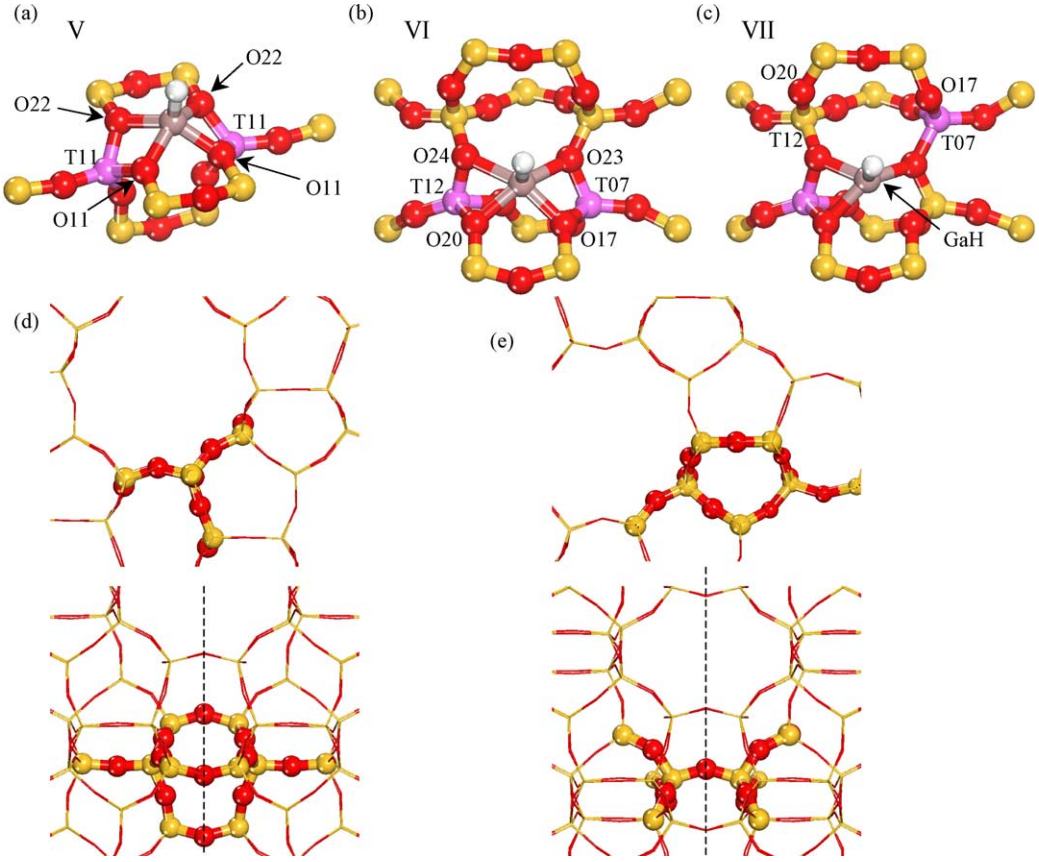

Fig. 2. Three-different sites for $Z^{2-}[GaH]^{2+}$-type: (a) six-membered ring with Al–Al distance of 4.529 Å, (b) eight-membered ring with Al–Al distance of 4.603 Å, (c) eight-membered ring with Al–Al distance of 5.534 Å, (d) two views of the location of the six-membered ring in the MFI structure and (e) two views of the location if the eight-membered ring in MFI structure.

clusters VI and VII. However, Al substitution at only one of the T12 (or T07) site breaks the symmetry. We substituted Si with Al at the T12 and T07 positions in these clusters. Although Al substitution was carried out at the same T positions, these two structures (VI and VII) are symmetrically non-equivalent geometries out of the four possible combinations for Al pair substitution. In the relaxed cluster (structure VI), the distance between the two Al atoms was 4.60 Å. We found that Ga coordinates with four lattice oxygen atoms in a square planar fashion. The Ga–O distance varied from 2.04 to 2.23 Å, while the Ga–H bond distance (1.54 Å) is slightly longer than that for site V.

To study the effect of the position of Al atoms in the ring, we have studied an alternative cluster (VII) with $[Ga–H]^{2+}$ species sitting in the same eight-membered ring. However, the Al pair in this model occupied the T12 and T07 positions (shown in Fig. 2) with a relaxed Al–Al distance of 5.53 Å. In this case, the gallium species was mainly coordinated with three-lattice oxygen having Ga–O distances from 2.04 to 2.14 Å. Important geometry and charge parameters of all seven-site models are listed in Tables 1 and 2. In this study, we considered Al substitution at different T sites like T12, T11 and T07. Schroder et al. [43] have used an ion-shell pair potential model to simulate the Al location at different framework positions. That study indicated a possibility of the random distribution of the framework Al due to narrow energy distribution among these structures. A similar conclusion was also drawn by Ricchiardi and Newsam [44] using force field methods. In the cluster models with two Al sites, Al substitutions are made in accordance with Lowenstein's rule, which forbids the Al substitution on neighboring T sites.

Our calculations were conducted using a double zeta 6–31g (d,p) basis set [45]. For gallium, this basis set corresponds to the compact contracted basis set by Binning and Curtiss [46] with d-polarization, and it has different structure than the traditional 6–31g basis set. For non-transition elements in the third row, mainly s- and p-type functions are involved in the bonding. However, the importance of the d-functions in the geometry optimization [47,48] necessitates the presence of the d-polarization functions for the Ga basis set. Recently a true 6–31g basis set for third row elements [48] was put forth, although its performance is equivalent to the one by Binning and Curtiss [46].

We have used a Becke three-parameter hybrid functional [49] (B3LYP) for this study. Previous work by Frash and van Santen [37] on the same system showed that this level of theory is adequate to draw consistent comparisons between different mechanisms. All of our calculations were done using the Gaussian03 program package [50]. Transition states were calculated using the quadratic synchronous transit (QST) method [51]. Validity of the critical transition states was confirmed using (1) imaginary frequency mode visualization, (2) relaxation by perturbing transition states along the imaginary frequency mode and (3) rigorous internal reaction coordinate (IRC) [52] relaxation. All the reported energies are corrected for zero point energy (ZPE) by doing normal mode analysis of the intermediates along the reaction paths. The inaccurate normal modes due to the frozen atoms in the cluster calculations are projected out of the Hessian to have consistent ZPE correction for a particular reaction path. The basis set superposition error (BSSE) was neglected, while calculating energetics for different mechanisms. A larger triple zeta (e.g. 6–311g) basis set will reduce [53] the basis set superposition error. The popular counterpoise method by Boys and Bernardi [54] can be used to estimate the BSSE; however, this often leads to the overestimation of the error [53]. For both stable intermediates and transition states, default convergence criteria of 0.00063 Å for average displacement and 0.35 kcal/Å for average gradient was employed. Although these criteria are very strict for real world applications, they ensure the reproducibility and reliability of the calculations for future studies.

Table 2
Comparison of the geometry and charge parameters of four $Z^{2-}[GaH]^{2+}$ species with two Al in six-membered ring (V), eight-membered ring with Al pair along the channel (VI) and eight-membered ring with Al pair across the channel surface (VII)

	V	VI	VII
Ga–H1 Å	1.531	1.541	1.530
Ga–O Å	2.014 (Ga–O11)[c]	2.042 (Ga–O17)[c]	2.272 (Ga–O17)
Ga–O Å	2.014 (Ga–O11)	2.102 (Ga–O23)	2.042 (Ga–O23)
Ga–O Å	2.030 (Ga–O22)	2.146 (Ga–O20)	2.141 (Ga–O20)
Ga–O Å	2.030 (Ga–O22)	2.226 (Ga–O24)	2.051 (Ga–O24)
Al–Al Å	4.528 (T11–T11)	4.603 (T12–T07)	5.534 (T12–T07)
Charge on Ga[a]	0.777	0.644	0.591
ΔH_0 (kcal/mol)[b]	27.88	0.15	−19.57

[a] Mulliken charge on the atom.
[b] Heat of reduction for reaction $Z^{2-}[GaH]^{2+} + H_2 \Leftrightarrow Z^{-}[HGaH]^{+} + Z^{-}H^{+}$ at 298.15 K and 1 atm.
[c] For oxygen naming in structures V and VI refer to Figs. 7 and 8, respectively.

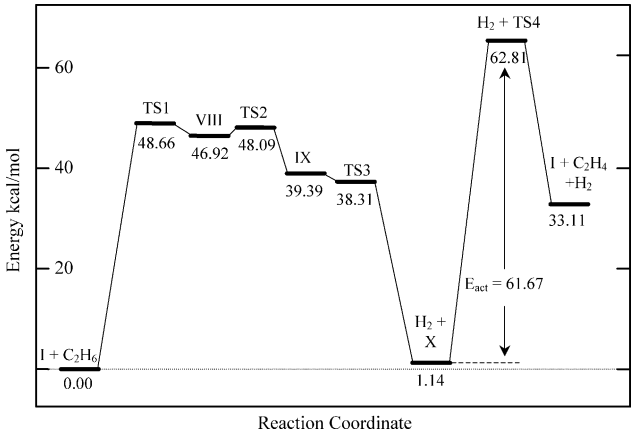

Fig. 3. Reaction path for the 'alkyl activation' mechanism of dehydrogenation of the ethane on $Z^{-}[HGaH]^{+}$ species (I) (all energies reported are after zero point energy correction).

3. Results and discussion

To carry out a consistent comparison between several dehydrogenation mechanisms, we first investigated the alkyl activation pathway proposed by Frash and van Santen [37] using a larger cluster model (11 T cluster, site I) of the catalytic site than their original work. We find that the activation energy for initial C–H activation is substantially higher (48.66 kcal/mol) compared to their previously calculated [37] value of 37.9 kcal/mol. We attribute the higher activation barrier to greater steric hindrance for C–H insertion caused by the constrained geometry of our cluster model. We have also located an additional transition state (TS2) for the rotation of the tetrahedral [$H_2GaC_2H_5$] species.

The energetics for this mechanism is given in Fig. 3 with geometry and charge parameters listed in Table 3. The O24–H3 distances in the structures VIII and IX indicate the formation of the Brønsted acid site during the reaction path. Simultaneously, the Mulliken charge on the Ga is very close to zero. The structure VIII (as shown in Fig. 4) could be formed by adsorption of the $H_2GaC_2H_5$ species on the Brønsted acid site. The adsorption energy we calculated for this transformation was 16.87 kcal/mol, indicating the strong binding for this intermediate.

The stable intermediate in C–H activation proceeds through rotation of the tetrahedral Ga species about the Ga–O20 coordination (process VIII → TS2 → IX in Fig. 4). As shown in Fig. 3, we observed very weakly activated transition states for this rotation followed by the removal of a H_2 molecule (process IX → TS3 → X + H_2 in Fig. 4). For TS3 in particular, the zero point energy correction was actually larger than the non-corrected activation energy (which within transition state theory corresponds to a net negative Gibbs free energy change at the transition state). We indicated this in Fig. 3 as a negative (ZPE corrected) activation barrier, which can be interpreted as essentially an unactivated process.

Table 3
Geometry and charge parameters of the intermediates along the dehydrogenation reaction path at $Z^-[HGaH]^+$ catalytic sites by 'alkyl activation mechanism'

	TS1	VIII	TS2	IX	TS3	X	TS4
Ga–O24 (Å)	2.759	2.959	3.026	3.076	3.054	1.982	1.992
Ga–O20 (Å)	2.032	2.105	2.113	2.084	2.048	2.014	2.131
Ga–H1 (Å)	1.571	1.583	1.597	1.641	1.689	–	–
Ga–H2 (Å)	1.563	1.572	1.567	1.570	1.567	1.562	1.555
Ga–H3 (Å)	2.028	2.342	2.229	2.240	2.137	–	–
Ga–H4 (Å)	–[b]	–	–	–	–	3.156	1.698
C1–H3 (Å)	1.490	2.077	2.380	3.053	–	–	–
C1–Ga (Å)	2.120	2.026	2.018	1.981	1.997	1.973	2.122
C2–H4 (Å)	–	–	–	–	–	1.094	1.788
O24–H3 (Å)	1.180	0.992	0.981	1.067	1.203	–	–
H1–H3 (Å)	–	–	2.086	1.184	0.991	–	–
C1–C2 (Å)	1.536	1.537	1.536	1.536	1.536	1.536	1.409
Charge on Ga[a]	0.178	0.084	0.062	0.233	0.268	0.508	0.346
Charge on C1[a]	−0.484	−0.408	−0.391	−0.335	−0.344	−0.352	−0.361
Charge on C2[a]	−0.313	−0.311	−0.315	−0.128	−0.337	−0.327	−0.165

[a] Mulliken charge on the atom.
[b] Not reported since not related to the relevant geometry transformation.

The activation barrier for the 'alkyl desorption' (process X → TS4 in Fig. 3) was 61.67 kcal/mol, which is in close agreement with the previously reported [37] value of 60.7 kcal/mol. This close agreement reflects the fact that the hydrocarbon species has very little interaction with the zeolite framework for this step of the mechanism. This high activation barrier for the alkyl removal step should lead to very low intrinsic reaction rate for the alkyl activation mechanism. This illuminates the essential problem with our understanding of C–H activation that current computational studies have yet to adequately explain the relatively low experimental [20] activation energy of 39 kcal/mol. We conclude from the

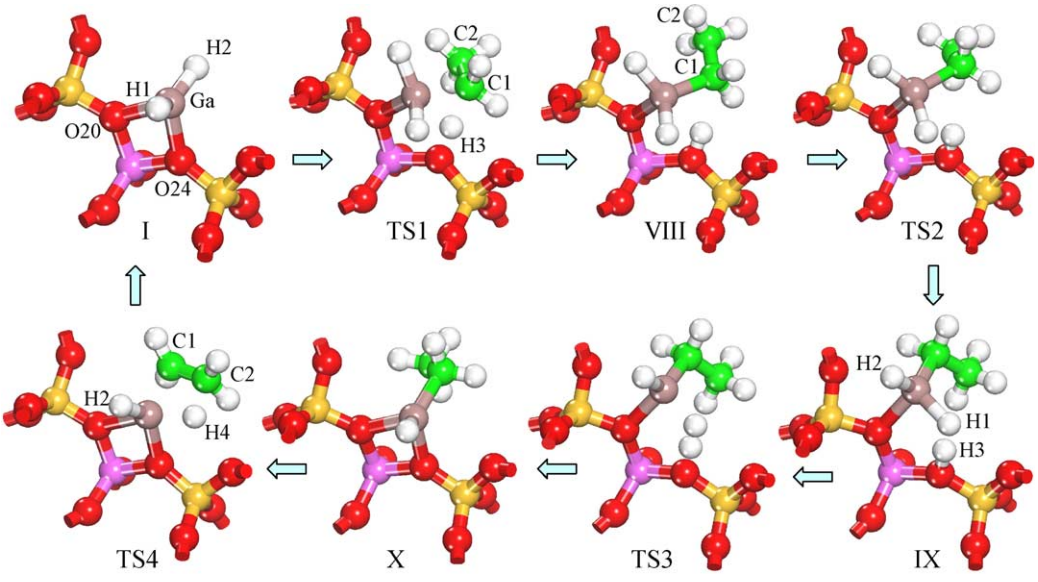

Fig. 4. Molecular transformations during dehydrogenation of ethane on $Z^-[HGaH]^+$ site (terminal SiH_3 are not shown for clarity).

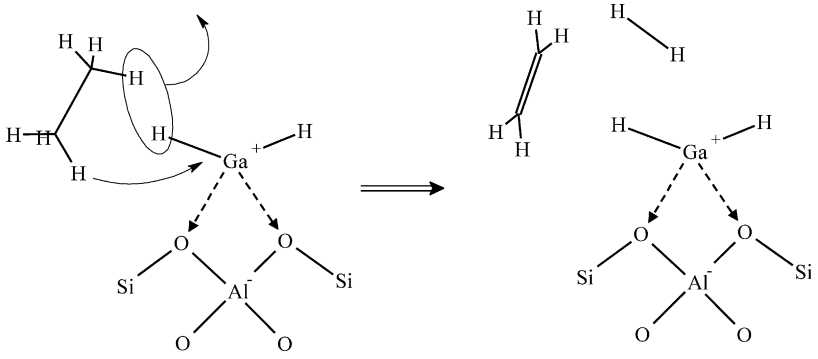

Scheme 1. Direct (one-step) dehydrogenation mechanism for ethane.

previous literature, and from our extension here, that the single site, $[HGaH]^+$, model does not represent the true mechanism for Ga-assisted dehydrogenation.

3.1. Direct dehydrogenation mechanism

In light of this conclusion, we investigated several other options, including the possibility of a direct (one-step) dehydrogenation of the hydrocarbon on a $Z^-[HGaH]^+$ species. As shown in Scheme 1, hydrogen from one of the alkane carbons combines with hydrogen from the active Ga-site to form molecular hydrogen. At the same time the hydrogen from the β-carbon replenishes the Ga–H coordination. Thus, in one-step there is a formation of an alkene and molecular hydrogen, and at the same time the catalytic site is regenerated.

Direct dehydrogenation involves breaking two C–H and one Ga–H bond with the simultaneous formation of H–H and Ga–H bonds. In addition the C–C bond length decreases with a C–C π-bond formation. In Fig. 5, we show the potential energy diagram for direct dehydrogenation for ethane, propane and *n*-butane. The comparison of the geometry parameters for transition states is reported in Table 4. The geometry parameters for all the transition states

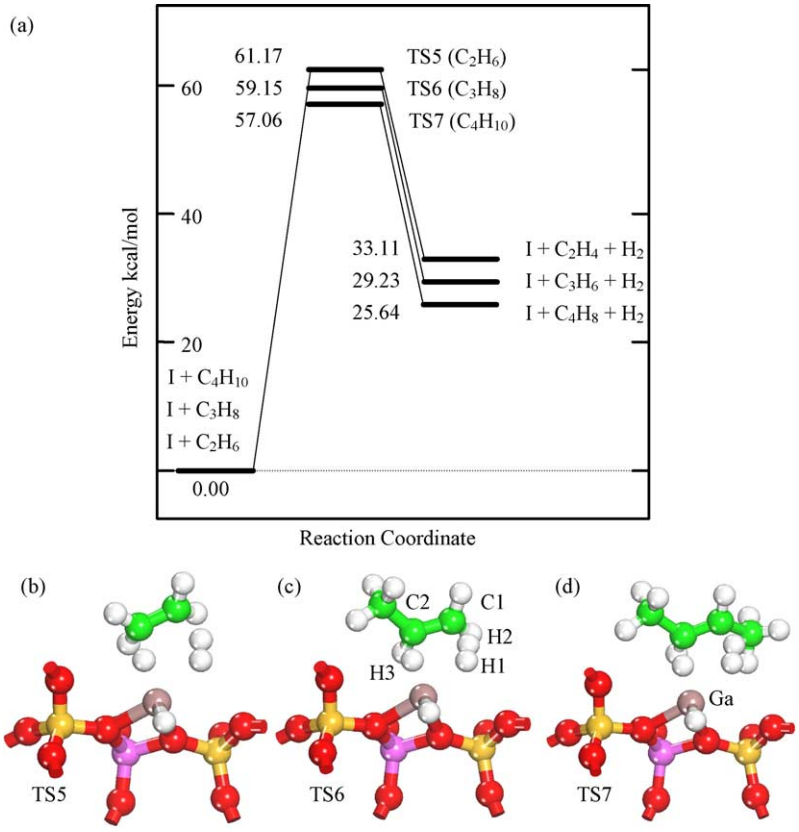

Fig. 5. Direct (one-step) dehydrogenation of light alkanes on the $Z^-[HGaH]^+$: (a) reaction path; transition state geometries for (b) ethane, (c) propane and (d) *n*-butane giving trans-2-butene (terminal SiH_3 groups were neglected for clarity).

Table 4
Comparison of the geometry and charge parameters of the transition states of direct (one-step) dehydrogenation at $Z^-[HGaX]^+$ catalytic sites

	TS5	TS6	TS7	TS8	TS9	TS10
X	H	H	H	CH3	OH	Cl
Alkane Cn	C2	C3	C4	C3	C3	C3
Ga–X (Å)	1.572	1.569	1.574	1.980	1.830	2.200
Ga–O24 (Å)	1.994	2.001	2.003	2.010	1.994	1.983
Ga–O20 (Å)	2.045	2.053	2.052	2.056	1.994	2.012
Ga–H1 (Å)	2.073	2.001	2.060	2.045	2.006	2.056
Ga–H3 (Å)	1.697	1.676	1.709	1.702	1.675	1.691
H1–H2 (Å)	0.834	0.852	0.843	0.850	0.840	0.829
C1–H2 (Å)	1.657	1.586	1.606	1.598	1.619	1.652
C2–H3 (Å)	1.435	1.494	1.431	1.447	1.466	1.436
C1–C2 (Å)	1.391	1.394	1.401	1.398	1.394	1.394
Charge on Ga[a]	0.447	0.422	0.416	0.554	0.668	0.528
Charge on H_2[a]	−0.011	0.006	−0.005	−0.011	−0.004	0.013
Charge on $C_n^{=}$[a]	0.000	0.020	0.029	0.000	0.048	0.059
E_{act} (kcal/mol)[b]	61.17	59.15	57.06	58.51	57.39	56.13

[a] Mulliken charges on the atom.
[b] Activation energy for the direct dehydrogenation mechanism.

were very similar. The total Mulliken charge on the individual fragments (H_2, C_nH_{2n}, $Z^+[HGaH]^-$) in the transition state structures were nearly zero. Similarly, we observed very small individual charges on the hydrogen atoms involved in the geometry transformation. We also observe the activation barrier for dehydrogenation decreases with the presence of the secondary carbon. This was expected since the secondary carbon has higher tendency to donate H compared to the primary carbon. The activation barrier for *n*-butane is about 4 kcal/mol lower compared to that of the ethane. This trend agrees with the experimental finding [26] that dehydrogenation of the higher alkanes (C4) is easier than that of lower alkanes (C2).

We note that the second hydrogen from the gallium dihydride extra-framework species is not involved in the reaction. Hence, to study the effect of the charge on the gallium atom on the activation barrier for the direct dehydrogenation path, we replaced this hydrogen with methyl (−CH_3), hydroxyl (−OH) and chlorine (−Cl)—designated generically as X. From Table 1, we show that the charge on the Ga is proportional to the electronegativity of the bonded constituent X. In Table 1, we listed heats of reaction for removal of X using H_2. We find that reduction of $Z^-[HGaX]^+$ is endothermic when X is OH or Cl. Thus, the presence of these species is quite possible under reaction conditions unless an elaborate reduction procedure is used for catalyst pretreatment. At the same time, direct dehydrogenation on these catalytic sites yields lower activation barriers. Thus, more electronegative species introduce a polar environment around the gallium, which

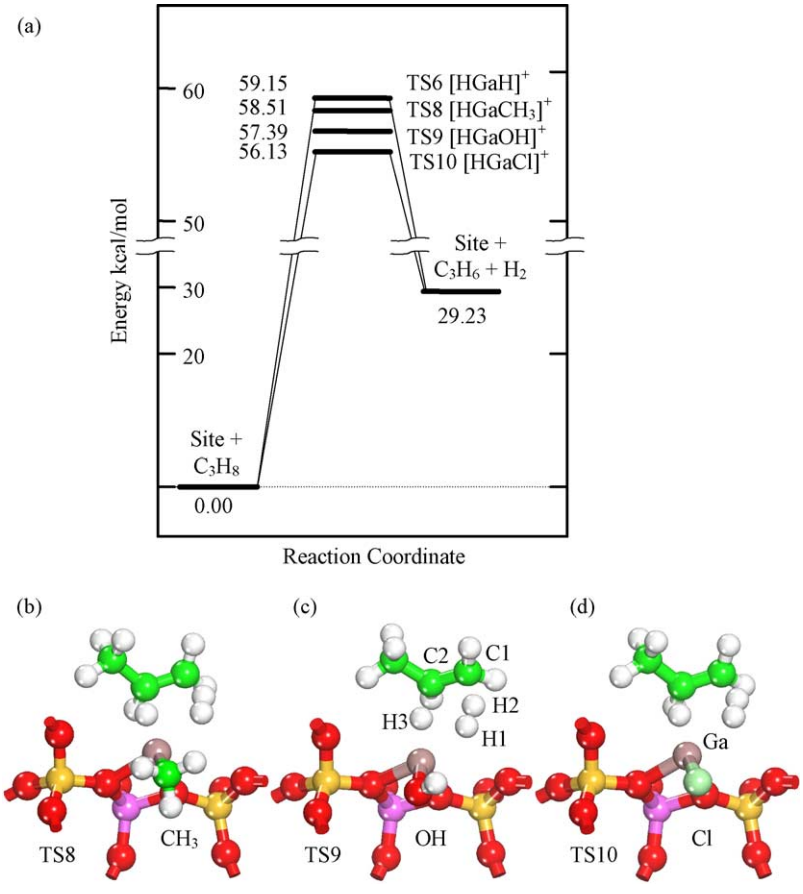

Fig. 6. Direct dehydrogenation of the propane on the $Z^-[HGaX]^+$: (a) reaction path; transition state geometries for (b) X = CH_3, (c) X = OH and (d) X = Cl.

facilitates the bond breaking and formation process. This results is in agreement with experimental results [19], which, starting from $GaCl_3$-impregnated HZSM-5, reports higher initial activity for propane aromatization.

Geometries of the transition states and the reaction path for direct dehydrogenation of propane on different $[HGaX]^+$ species are shown in Fig. 6. The activation energy for $[HGaCl]^+$ is 56.13 kcal/mol, which is lower than that for $[HGaH]^+$ (59.15 kcal/mol). However, we like to note that the activation barrier for dehydrogenation by the direct dehydrogenation mechanism (61.17 kcal/mol) is similar to the highest barrier for the 'alkyl activation reaction path' discussed above. Once again, we are forced to conclude that both direct activation on the reduced ($[HGaH]^+$) single site as well as alternatively ligated single $[HGaX]^+$ sites, are not correct representations of the true C–H activation pathway.

3.2. Carbenium activation pathway for $Z^{2-}[GaH]^{2+}$ species

Examining the mechanism above (Fig. 3), we observe that during alkyl activation, the alkene desorption step (process X → TS4) faces a very high activation energy (as high as 61.67 kcal/mol). Based on the work by Frash and van Santen [37] and our subsequent extension presented above, we conclude that for $Z^-[HGaH]^+$ sites, it will generally be very difficult, if not impossible, to find a reaction path with low enough activation barriers to match experimental results [20]. At the same time, our results in the previous section indicate that a polar environment around the Ga species can have significant effect on reaction energetics. What we show now is that the polarity of the Ga–O coordination can be enhanced by placing Ga species in the vicinity of two Al T sites.

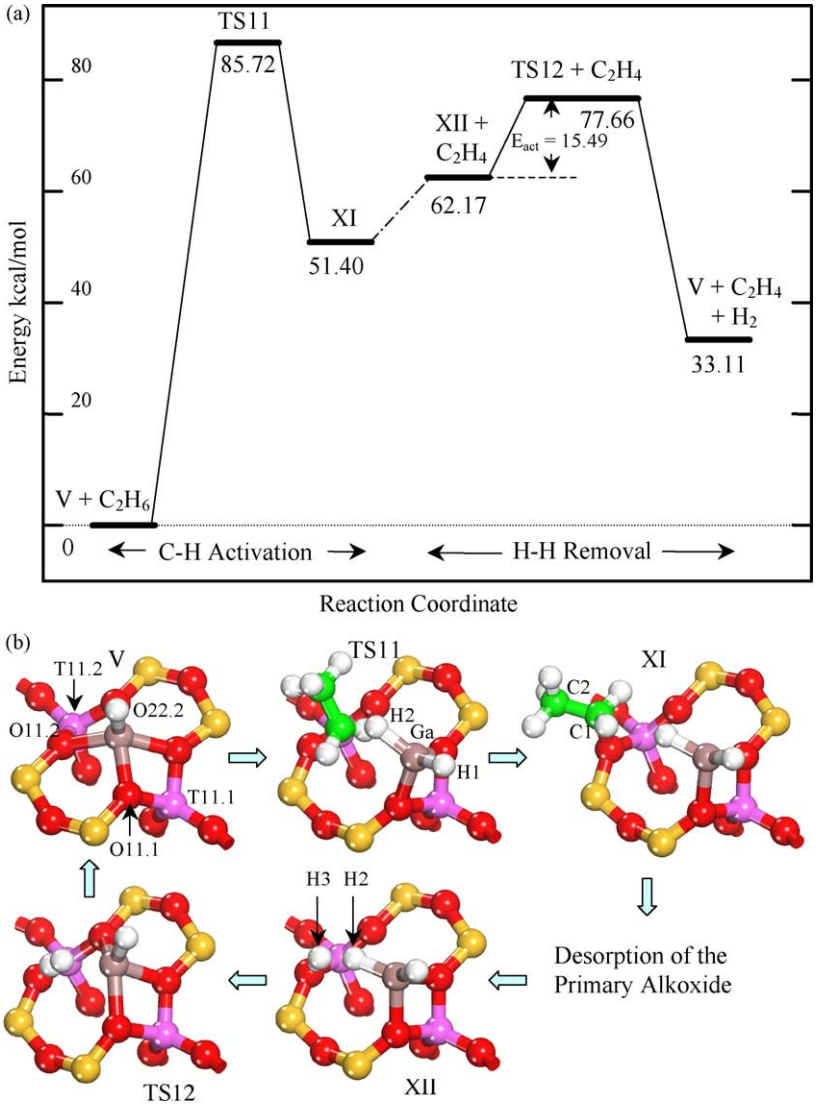

Fig. 7. Carbenium activation path of ethane dehydrogenation on $Z^{2-}GaH^{2+}$ species (V) in six-membered ring: (a) reaction path consisting two-distinct steps and (b) geometry transformations during dehydrogenation path (naming convention for oxygen to define geometry parameters in Table 5).

In an attempt to find a catalytic environment, which better facilitates alkene desorption, we considered three-different sites for this study. The first active site represents an 'α-type' site as per the classification of pair sites by Dedecek et al. [55] These sites consist of a pair of five-membered rings fused to form a slightly elongated six-membered ring. As shown in Fig. 2a, the gallium species $[GaH]^{2+}$ sits at the center of the rectangle of the four oxygen atoms. The Ga–O distance is about 2.02 Å with significant positive charge on gallium. In Table 2, we provide the geometry and charge parameters for all sites considered containing pairs of Al.

The bare gallium mono-hydride site can be reduced using H_2 to form a regular gallium di-hydride and Brønsted acid site. For the 'α-type' site (V), we found this reaction (process $V + H_2 \rightarrow XII$) to be endothermic with 27.88 kcal/mol heat of reaction. We will, hence forth, refer to this as ''H_2 site-reduction'' and designate the heat of this reaction as ΔH_{red}. The stability of the $[GaH]^{2+}$ species, signified by the endothermic heat of H_2 site-reduction, is in agreement with the similar results for Zn^{2+} species by Shubin et al. [56] and Barbosa et al. [57] Thus, at lower temperature most of the 'α-type' sites will be in the dehydrogenated form as described above.

Our investigation of the carbenium activation mechanism consists of three-distinct steps: (1) activation of the C–H bond and formation of an alkoxide like intermediate, (2) removal of the primary alkoxide by desorption of an alkene and (3) desorption of molecular hydrogen to complete the catalytic cycle. For the α-type site (V), we report the reaction path for carbenium activation in Fig. 7a. We have limited our investigation only to the activation of the C–H bond and removal of dihydrogen to regenerate the active site. Desorption of an alkene starting from the primary alkoxide has been extensively studied [58,59], and the activation barrier for this process should be about 35–40 kcal/mol.

For catalytic site V, we find the energy barrier for C–H activation is 85.72 kcal/mol, corresponding to the initial alkane adsorption and hydrogen removal. Schematically, the $[GaH]^{2+}$ species is responsible for removing hydrogen from the alkane during this step, forming the traditional $[HGaH]^{+}$ moiety residing on one of the Al atoms. The alkyl species subsequently adsorbs as an alkoxide near the second Al. The activation barrier for this step (process $V + C_2H_6 \rightarrow$ TS11 in Fig. 7) is very high considering the other reaction paths we have presented so far. The transition state geometry (structure TS11 in Fig. 7) for C–H activation shows the sp^2 hybrid character of the carbon involved. As the tetrahedral carbon looses one of its hydrogens to gallium, it inverts to adsorb as an alkoxide on the opposite framework oxygen. This mechanism can be visualized as a sn2 attack by framework oxygen (conjugate base of the Brønsted acid site) on the tetrahedral carbon center. In Table 5, we list the geometry and charge parameters for all the species along the catalytic cycle. In the transition state (TS11), the hydrocarbon species carries more positive charge as electrons

Table 5
Geometry and charge parameters of the intermediates along the dehydrogenation reaction path at $Z^{2-}[GaH]^{2+}$ catalytic site (V) via 'carbenium activation mechanism'

	V[a]	TS11	XI	XII	TS12
Ga–O11.1 (Å)	2.014	1.965	1.995	1.984	2.135
Ga–O22.1 (Å)	2.030	1.955	1.982	1.972	1.935
Ga–O11.2 (Å)	2.014	4.501	4.256	3.872	2.984
Ga–O22.2 (Å)	2.030	4.160	3.772	3.538	2.112
Ga–H1 (Å)	1.531	1.546	1.553	1.549	1.548
Ga–H2 (Å)	–[c]	1.617	1.556	1.573	1.730
C1–H2 (Å)	–	1.733	2.807	–	–
C1–O11.2 (Å)	–	2.129	1.503	–	–
O11.2–H3 (Å)	–	–	–	0.980	1.285
H2–H3 (Å)	–	–	–	1.794	0.919
Charge on Ga[b]	0.777	0.529	0.446	0.508	0.580
Charge on C1[b]	−0.315[c]	−0.106	0.034	–	–
Charge on H2[b]	0.105[d]	−0.048	−0.063	−0.125	−0.045
Charge on H3[b]	–	–	–	0.382	0.243

[a] For oxygen naming refer to Fig. 7.
[b] Mulliken charge on the atom.
[c] Not reported since not related to the geometry transformation.
[d] Mulliken charges for gaseous ethane molecule.

populate the covalent bond between the H and Ga. The gallium dihydride formed in this process is similar to the active site discussed in the previous sections. Ethene subsequently desorbs from the primary alkoxide, leaving behind the Brønsted acid site.

We observe strong hydrogen bonding between the Brønsted proton and the hydridic hydrogen in structure XII (Fig. 7b). Due to this interaction, the Brønsted proton bends out of plane by an angle of 37.8°. Also, the positive charge on the proton induces a small negative charge on the hydridic hydrogen. This polarization helps hydrogen removal step, which has an activation barrier of only 15.49 kcal/mol. The Ga–H stretching frequency (1914 cm^{-1}) for the polarized Ga–H bond is markedly lower than the non-polar Ga–H bond (1995 cm^{-1}). However, we note that the activation barrier for reverse reaction (H_2 adsorption) is rather high (44.55 kcal/mol), which makes the site kinetically stable (less active). We observe that the activation barrier for hydrogen removal is substantially smaller than that for C–H activation. The activation barrier for C–H activation is directly related to the large endothermicity of the C–H activation step (ΔE = 51.40 kcal/mol).

The other two cluster models containing two Al T sites (VI and VII), represent the γ-type site according to the classification by Dedecek et al. [55]. Model VI consists of two five-membered rings connected by a four-membered ring. This site is located along the walls of the sinusoidal channel near the cross-section of the straight and the sinusoidal channel. Comparing Al–Al distances in the relaxed models, we find 4.60 Å for structure VI (Fig. 2) compared to 5.53 Å for structure VII (Fig. 2). Qualitatively, the Al pair was placed parallel to the sinusoidal channel for site VI and for site VII it was placed diagonally along the channel surface. The heats of H_2 site-reduction (ΔH_{red}) for these two models (processes VI → XV and VII → XVIII)

were 0.15 and −19.57 kcal/mol (Table 2), respectively. Thus, the process of forming Brønsted acid/gallium dihydride pairs is thermo-neutral for site VI and exothermic for site VII; suggesting that the $[GaH]^{2+}$ species are less stable in larger eight-membered ring structures. However, our reported energies of reaction for H_2 site-reduction make the presence of both $[GaH]^{2+}$ and $[HGaH]^{+}$ species feasible under normal reaction conditions. Since structures VI and VII represent the same silicalite framework and have same stoichiometry, we can directly compare the total energy for these structures. We find VI is more stable compared to structure VII by 12.55 kcal/mol. Considering the narrow energy distribution for framework substitution at different T sites, this stability could be attributed to the optimum coordination of the $[GaH]^{+}$ species with framework oxygen atoms in case of structure VI. After reduction by H_2 (after the formation of the Brønsted acid site and $Z^{-}[HGaH]^{+}$ pair) the stability order is reversed. We find structure XVIII more stable compared to XV by only 3.68 kcal/mol. This small difference in the energies is expected as the Brønsted proton and $[HGaH]^{+}$ occupy crystallographically equivalent positions (T12 and T07) individually in XV and XVIII. However, these structures are symmetrically non-equivalent as explained in Section 2.

In Fig. 8, we report the energetics of the carbenium activation mechanism for site VI. We found that the C–H activation part consists of two steps. In the first step (process VI → XIII in Fig. 8), the Ga–O coordination opens such that Ga is coordinated with only two framework oxygens (O17 and O23). The coordinatively unsaturated GaH species is partially satisfied by the methyl group of ethane as shown in the structure XIII (Fig. 8b). In this structure we observed an increase in the negative charge on the primary carbon (C1)

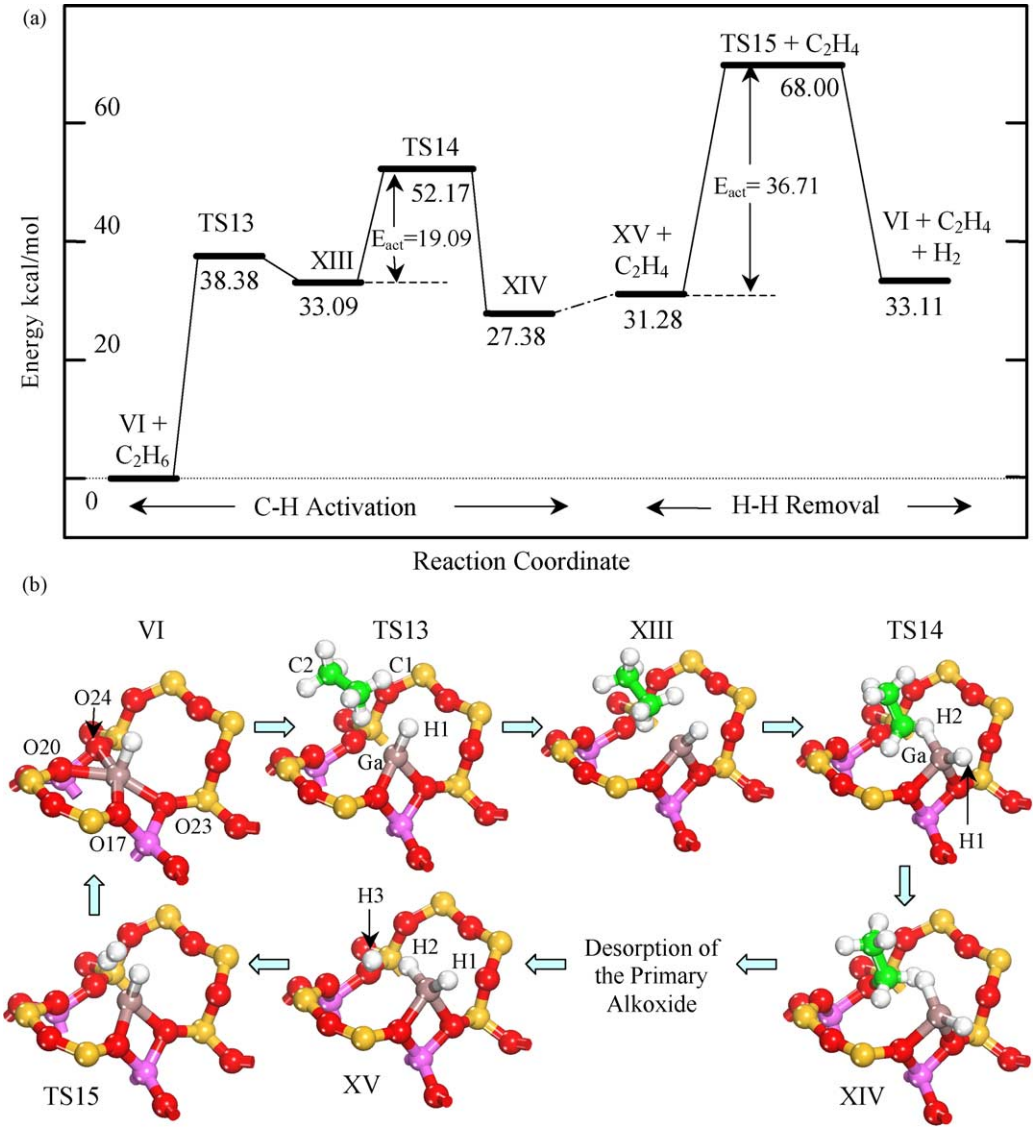

Fig. 8. Carbenium mechanistic path of ethane dehydrogenation on $Z^{2-}[GaH]^{2+}$ site (VI) with two Al atoms located in the eight-membered ring: (a) reaction path consisting two-distinct steps and (b) geometry transformations during dehydrogenation reaction path (naming convention for oxygen to define geometry parameters in Table 6).

and an increase in the positive charge on the hydrogen bonded to it. Thus, the C–H bonds of the methyl group become much more polar during insertion. This adsorption reaction (process VI → TS13 → XIII in Fig. 8) is activated by 38.38 kcal/mol. After the insertion, the methyl group slightly rotates, loosing hydrogen to form $[HGaH]^+$ species and adsorbs itself as an alkoxide. The transition state for this second step (process XIII → TS14 → XIV in Fig. 8) is activated by 19.09 kcal/mol. As discussed previously the transient geometry has sp^2 carbon character, which undergoes sn2 inversion. The presence of the intermediate (structure XIII) during the C–H activation process is kinetically significant. It should enhance the dehydrogenation rate by reducing the apparent activation energy. However, the lower stability of the $[GaH]^{2+}$ species results in a penalty for the hydrogen removal process. In this model, the hydrogen removal step (process XV → TS15 → VI+H_2 in Fig. 8) is activated by 36.71 kcal/mol, but overall, the current catalytic site (structure VI) should have better dehydrogenation activity compared to the 'α-type' site discussed previously. In Table 6, we listed the geometry and the charge parameters for all the intermediates along this reaction path.

A similar reaction path for 'γ-type' site with different Al positions (VII) is shown in Fig. 9. The exothermic dissociative adsorption of H_2 (Table 2) indicates that this catalytic site is more active than the models V and VI. Hence, the C–H dissociation reaction faces a very low energy barrier. In model VII, the two-step process of dissociative adsorption of ethane has activation energies of

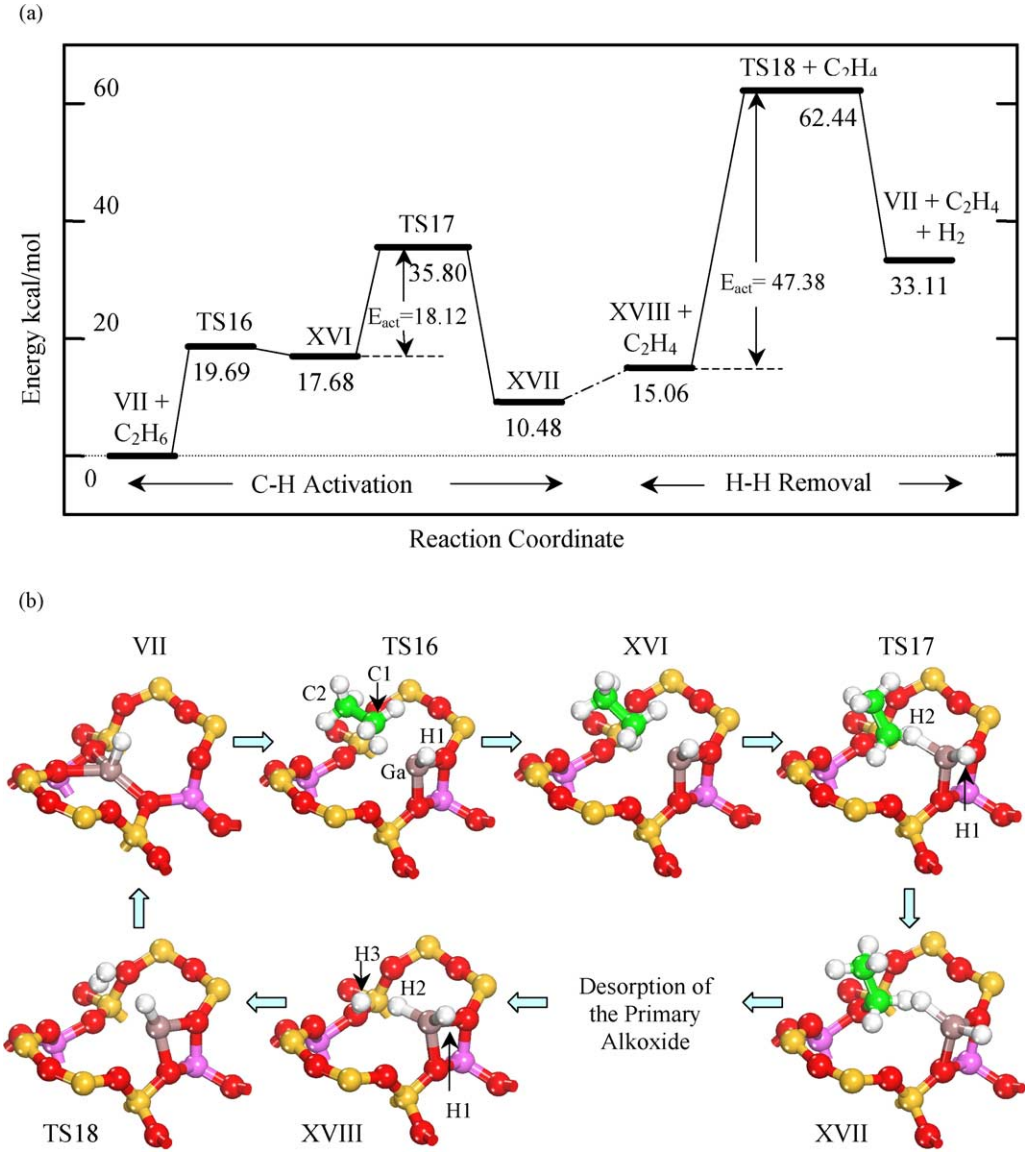

Fig. 9. Carbenium activation path of ethane dehydrogenation on $Z^{2-}[GaH]^{2+}$ site (VII) with two Al atoms located in the eight-membered ring: (a) reaction path consisting two-distinct steps and (b) geometry transformations during dehydrogenation reaction path.

Table 6
Geometry and charge parameters of the intermediates along the dehydrogenation reaction path at $Z^{2-}[GaH]^{2+}$ catalytic site (VI) via 'carbenium activation mechanism'

	VI[a]	TS13	XIII	TS14	XIV	XV	TS15
Ga–O17 (Å)	2.043	1.897	1.905	1.964	2.000	1.998	1.908
Ga–O23 (Å)	2.102	1.892	1.886	1.943	1.989	1.982	1.937
Ga–O24 (Å)	2.226	3.447	4.451	4.787	4.996	4.261	2.891
Ga–O20 (Å)	2.146	3.432	4.429	4.790	5.171	4.244	3.163
Ga–H1 (Å)	1.541	1.523	1.529	1.541	1.553	1.549	1.532
Ga–H2 (Å)	–[c]	–	–	1.613	1.558	1.570	2.125
Ga–C1 (Å)	–	2.959	2.332	2.974	3.750	–	–
C1–H2 (Å)	–	1.096	1.103	1.650	2.787	–	–
C1–O24 (Å)	–	3.241	3.161	2.116	1.494	–	–
O24–H3 (Å)	–	–	–	–	–	0.973	1.743
H2–H3 (Å)	–	–	–	–	–	2.182	0.777
Charge on Ga[b]	0.644	0.685	0.594	0.563	0.427	0.427	0.696
Charge on C1[b]	−0.315[d]	−0.337	−0.465	−0.080	0.069	–	–
Charge on H2[b]	0.105[d]	–	–	−0.062	−0.057	−0.100	−0.032
Charge on H3[b]	–	–	–	–	–	0.388	0.105

[a] For oxygen naming refer to Fig. 8.
[b] Mulliken charge on the atom.
[c] Not reported since not related to the geometry transformation.
[d] Mulliken charges for gaseous ethane molecule.

19.69 kcal/mol (process VII + C_2H_6 → TS16 → XVI in Fig. 9) and 18.12 kcal/mol (process XVI → TS17 → XVII in Fig. 9), respectively. Thus, the activation barriers for the second step of C–H activation are similar for the sites VI and VII, and hence the activation barrier for the initial insertion of the methyl group in Ga–O coordination can be easily correlated to the stability of the site. The H_2 removal step (process XVIII → TS18 → VII + H_2 in Fig. 9) has significantly higher activation barrier of 47.38 kcal/mol compared to that for structure VI (36.72 kcal/mol). Thus, an increase in the Al–Al distance will further increase the H_2 removal activation barrier. Important geometry and charge

Table 7
Geometry and charge parameters of the intermediates along the dehydrogenation reaction path at $Z^{2-}[GaH]^{2+}$ catalytic site (VII) via 'carbenium activation mechanism'

	VII	TS16	XVI	TS17	XVII	XVIII	TS18
Ga–O17.2 (Å)	3.638	1.925	1.928	1.982	2.021	2.026	1.917
Ga–O23 (Å)	2.042	1.880	1.882	1.937	1.984	1.977	1.863
Ga–O24 (Å)	2.051	4.500	4.488	4.806	5.009	4.291	3.853
Ga–O20 (Å)	2.141	4.996	4.996	5.262	5.678	4.735	4.417
Ga–H1 (Å)	1.530	1.522	1.528	1.540	1.553	1.547	1.519
Ga–H2 (Å)	–[b]	–	–	1.612	1.557	1.569	3.029
Ga–C1 (Å)	–	2.534	2.331	2.975	3.747	–	–
C1–H2 (Å)	–	1.097	1.108	1.637	2.795	–	–
C1–O24 (Å)	–	3.755	3.150	2.120	1.494	–	–
O24–H3 (Å)	–	–	–	–	–	0.972	2.422
H2–H3 (Å)	–	–	–	–	–	2.187	0.749
Charge on Ga[a]	0.591	0.606	0.587	0.568	0.425	0.428	0.742
Charge on C1[a]	−0.315[c]	−0.382	−0.465	−0.083	0.071	–	–
Charge on H2[a]	0.105[c]	–	–	−0.058	−0.052	−0.096	−0.068
Charge on H3[a]	–	–	–	–	–	0.388	0.092

[a] Mulliken charge on the atom.
[b] Not reported since not related to the geometry transformation.
[c] Mulliken charges for gaseous ethane molecule.

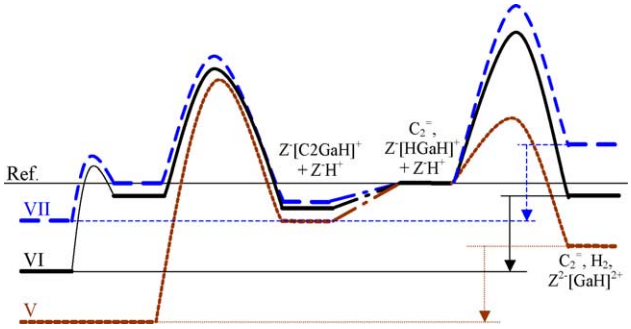

Scheme 2. A schematic representation of the reaction path energetics for three-$Z^{2-}[GaH]^{2+}$ sites: (- - -) site V, (—) site VI and (– – –) site VII.

parameters for the intermediates along this reaction path are reported in Table 7.

A schematic representation of the energetics for three-catalytic sites is shown in the Scheme 2. Catalytic sites XII, XV and XVIII, before the removal of hydrogen, consist of a Brønsted acid site and $[HGaH]^+$ species together. In the Scheme 2, we have shifted the energetics of all three-catalytic sites in such a way that the energies of the structures XII, XV and XVIII are aligned. Now, the relative energies of the species represent the relative activity or stability of the intermediates on individual scales. With our calculations we find that there is a natural optimum for the activity of the $Z^{2-}[GaH]^{2+}$ site. If it is too stable, like in model V for the six-membered ring, the initial activation of the C–H bond is very high, while regeneration of the catalyst site, and H_2 removal, has a lower activation barrier. On the other hand, if the catalyst site is very active, like in model VII for the eight-membered ring, then the C–H activation barrier is very low. However, the regeneration of the same active catalyst site by H_2 removal faces a higher activation barrier.

On closer examination of the Scheme 2, the Brønsted–Evans–Polanyi relations seems applicable for both C–H activation and H_2 removal steps as ΔH_{red} and E_{act} are clearly correlated for the individual steps. This concept of 'optimum activity of the catalyst site' is more popularly known as the Sabatier principle in the heterogeneous catalysis literature. In this particular case, we relate the activity directly to the catalyst site geometry. A simple correlation between the Al–Al distance and the activity for dehydrogenation can then be formulated. Another possibility is to formulate such correlations in terms of the stability if the $[GaH]^+$ species (ΔH_{red}) at the different extra-framework positions. As shown in Table 2, stability of the site can be quantified in terms of the heat of reaction for H_2 site reduction. In Fig. 10, we have plotted the important activation energies for both (i) C–H activation and (ii) H_2 removal against the ΔH_{red} for H_2 site reduction. For the thermo-neutral heat of reaction (model VI), we observe the optimum activity of the catalyst site. These kinds of correlations will provide simple structure–activity relations, which could be used to manipulate the dehydrogenation activity of the catalyst. Although our investigation indicates the extra-framework Ga in the

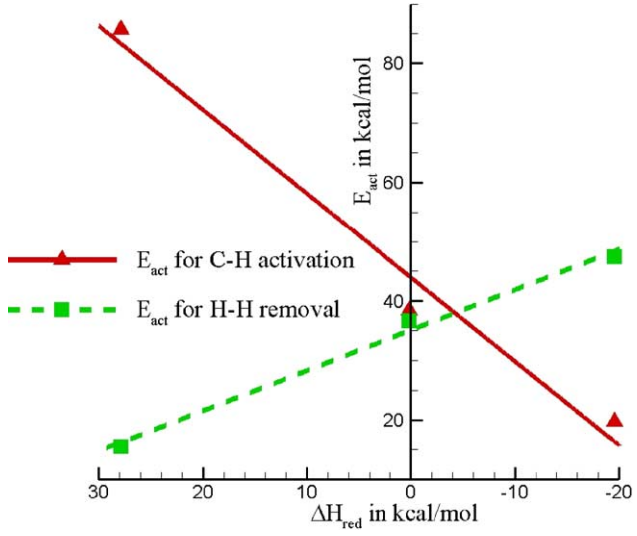

Fig. 10. Important activation energies plotted against the heat of reaction for dissociative adsorption of H_2 (i.e. Reduction of the $Z^{2-}[GaH]^{2+}$ species).

vicinity of the two-framework Al (rather than one Al site) should have higher activity, questions still remain about the probability of finding the Al pairs in high Si/Al zeolites. However, our results indicate that the Al pairs in larger (eight-membered) rings should give better dehydrogenation activity. A recent study by Gabova et al. [60] suggests that the fraction of the Al pair sites depends on the source of the Al. They point out that although the majority of the Al represents the isolated sites, depending on the source of the Al, the faction representing the Al pair sites can be as high as 27%. Dedecek et al. [40] reported a significant faction (∼45%) of Al existing as pair sites even at higher Si/Al ratio for a particular sample of ZSM-5. Although the statistical probability of finding pair Al sites assuming a random distribution is low for high Si/Al ratio zeolite, the actual probability is a strong function of the synthesis method. Industrially, the choice of high Si/Al ratio zeolites is influenced by the improved selectivity and lower deactivation of such material. Clearly, a further investigation is needed regarding the dehydrogenation activity of the Ga-HZSM-5 catalyst at different Si/Al ratio prepared using different synthesis procedures.

In Table 8, we report the Ga–H stretching frequencies (both 'as calculated' and 'scaled') for different structures. The recommended [61] scaling factor for the frequencies for the current level of theory [B3LYP/6-31g(d,p)] is 0.9614. We calculated a scaling factor of 0.9529 by comparing the experimental and calculated Ga–H frequency in GaH_3 gas phase molecule. After scaling, the Ga–H stretching frequencies for the $Z^{2-}[GaH]^{2+}$ catalytic sites match with the experimental [33] Ga–H stretching frequencies of 2041 and 2059 cm^{-1}. Although it is difficult to conclude these peaks correspond to $Z^{2-}[GaH]^{2+}$, since we expect relatively low concentration of the $[GaH]^{2+}$ moieties, the DRIFTS peaks are at least consistent with our $Z^{2-}[GaH]^{2+}$ Al-pair site model.

Table 8
Ga–H stretching frequencies for different intermediates

Structure	As calculated frequencies	Scaled frequencies[a]
I	2039[b]	1943[b]
	2077	1979
II	2091	1993
III	2090	1992
IV	2117	2017
V	2177	2074
VI	2134	2033
VII	2170	2068
XI	2014[c]	1919[c]
	2100	2001
XV	2024[c]	1929[c]
	2110	2011
XVIII	2034[c]	1939[c]
	2112	2013

[a] Scaling factor of 0.9529.
[b] Low frequency stretch corresponding to more polar Ga–H bond out of the two Ga–H bonds.
[c] Ga–H bond polarized by Brønsted acid site.

4. Conclusions

A one-step dehydrogenation path was investigated and the effects of alkane chain length, and the relative charge on the gallium in $Z^-[HGaX]^+$ catalyst site model were studied. We find the one-step dehydrogenation path, where several simultaneous bond scission and formation steps are involved, is favored by a polar environment surrounding Ga species. The activation barrier for the one-step dehydrogenation path is comparable with the maximum activation barrier for previously proposed alkyl mechanisms. However, activation barriers for all single-site GaH_2-based mechanisms result in activation energies that are much too high to reconcile experimental observations (activation energy of 39 kcal/mol). Thus, we conclude that a single site, $[HGaH]^+$, model does not represent the true mechanism for Ga-assisted dehydrogenation.

We subsequently investigated the possibility of alkane activation mechanisms by gallium species $[GaH]^{2+}$ in proximity to two aluminum T sites. Out of three-$Z^{2-}[GaH]^{2+}$ sites investigated, all with varying Al–Al distances, we find the gallium species in the six-membered ring represent the most stable site (highest ΔH_{red}). In models of eight-membered rings, larger Al–Al distances corresponded to lower site stability. The trends in reactivity show that higher site stability, and consequently smaller Al–Al distances, resulted in larger activation barriers for C–H activation (85.72 kcal/mol) and lower barriers for H_2 desorption and site regeneration (15.49 kcal/mol). Thus, we found an optimal Al–Al distance (4.53 Å) corresponding to a minimum overall barrier (38.38 kcal/mol for C–H activation and 36.71 kcal/mol H_2 removal) for dehydrogenation reaction as a result of the competition between these two trends. This competition between two trends exemplifies the

applicability of the Sabatier principle. We conclude that out of several possible catalytic sites in Ga-HZSM-5, extra-framework gallium species near pairs of tetrahedral Al have higher activity, and the activity of these sites can be correlated to Al–Al distance. We expect these results could be useful for systematic exploration of viable zeolite frameworks and site geometries in the interest of designing novel catalysts for alkane activation processes.

Acknowledgments

We thank Prof. W. Nicholas Delgass for enlightening discussions on zeolite catalyzed hydrocarbon chemistry. This work was supported by the State of Indiana through a grant from the 21st Century Technology Fund, US Department of Energy (DOE), Office of Basic Sciences: grant number DE-FG02-03ER-15466 and through the National Science Foundation grant # CTS-0238989-CAREER. Computational resources were obtained through a grant # MCA04N010 from the National Computational Science Alliance (Machines: copper.ncsa.uiuc.edu and tungsten.ncsa.uiuc.edu) and through supercomputing resources at Purdue University.

References

[1] G.L. Price, V. Kanazirev, K.M. Dooley, V.I. Hart, J. Catal. 173 (1998) 17.
[2] R. Fricke, H. Kosslick, G. Lischke, M. Richter, Chem. Rev. 100 (2000) 2303.
[3] H. Kitagawa, Y. Sendoda, Y. Ono, J. Catal. 101 (1986) 12.
[4] P. Meriaudeau, C. Naccache, J. Mol. Catal. 59 (1990) L31.
[5] P. Meriaudeau, G. Sapaly, C. Naccache, J. Mol. Catal. 81 (1993) 293.
[6] P. Meriaudeau, C. Naccache, J. Mol. Catal. 50 (1989) L7.
[7] P. Meriaudeau, M. Primet, J. Mol. Catal. 61 (1990) 227.
[8] P. Meriaudeau, C. Naccache, Appl. Catal. 73 (1991) L13.
[9] J.F. Joly, H. Ajot, E. Merlen, F. Raatz, F. Alario, Appl. Catal. A 79 (1991) 249.
[10] P. Meriaudeau, C. Naccache, J. Catal. 157 (1995) 283.
[11] N.S. Gnep, J.Y. Doyemet, A.M. Seco, F.R. Ribeiro, M. Guisnet, Appl. Catal. 43 (1988) 155.
[12] N.S. Gnep, J.Y. Doyement, M. Guisnet, in: H.G. Karge, J. Weitkamp (Eds.), Zeolites as Catalysts, Sorbents and Detergent Builders, Elsevier, Amsterdam, 1989, p. 153.
[13] E.G. Derouane, S.B. Abdul Hamid, I.I. Ivanova, N. Blom, P. Højlund-Nielsen, J. Mol. Catal. 86 (1994) 371.
[14] M. Barre, N.S. Gnep, P. Magnoux, S. Sansare, V.R. Choudhary, M. Guisnet, Catal. Lett. 21 (1993) 275.
[15] J.A. Biscardi, E. Iglesia, Catal. Today 31 (1996) 207.
[16] B.S. Kwak, W.M.H. Sachtler, J. Catal. 145 (1994) 456.
[17] B.S. Kwak, W.M.H. Sachtler, W.O. Haag, J. Catal. 149 (1994) 465.
[18] V.B. Kazansky, L.M. Kustov, A.Y. Khodakov, in: P.A. Future, R.A. Jacobs, van Santen (Eds.), Zeolites: Facts, Figures, Elsevier Science Publisher, Amsterdam, 1989, p. 1173.
[19] C.R. Bayense, J.H.C. van Hooff, Appl. Catal. A 79 (1991) 127.
[20] J. Bandiera, Y.B. Taarit, Appl. Catal. A 152 (1997) 43.
[21] V. Kanazirev, R. Dimitrova, G.L. Price, A.Y. Khodakov, L.M. Kustov, V.B. Kazansky, J. Mol. Catal. 70 (1991) 111.
[22] G.L. Price, V. Kanazirev, J. Catal. 126 (1990) 267.
[23] G.L. Price, V. Kanazirev, J. Mol. Catal. 66 (1991) 115.
[24] M. Guisnet, N.S. Gnep, F. Alario, Appl. Catal. A 89 (1992) 1.
[25] G. Giannetto, R. Monque, R. Galiasso, Catal. Rev. Sci. Eng. 36 (1994) 271.
[26] Y. Ono, Catal. Rev. Sci. Eng. 34 (1992) 179.
[27] J. Bandiera, Y. Bentaarit, Appl. Catal. 62 (1990) 309.
[28] T. Mole, J.R. Anderson, G. Creer, Appl. Catal. 17 (1985) 127.
[29] E. Iglesia, D.G. Barton, J.A. Biscardi, M.J.L. Gines, S.L. Soled, Catal. Today 38 (1997) 339.
[30] N.S. Gnep, J.Y. Doyement, M. Guisnet, J. Mol. Catal. 45 (1988) 281.
[31] R. Le Van Mao, L. Dufresne, Appl. Catal. 52 (1989) 1.
[32] G.D. Meitzner, E. Iglesia, J.E. Baumgartner, E.S. Huang, J. Catal. 140 (1993) 209.
[33] V.B. Kazansky, I.R. Subbotina, R.A. van Santen, E.J.M. Hensen, J. Catal. 227 (2004) 263.
[34] H. Himei, M. Yamadaya, M. Kubo, R. Vetrivel, E. Broclawik, A. Miyamoto, J. Phys. Chem. 99 (1995) 12461.
[35] E. Broclawik, H. Himei, M. Yamadaya, M. Kubo, A. Miyamoto, R. Vetrivel, J. Chem. Phys. 103 (1995) 2102.
[36] N.O. Gonzales, A.K. Chakraborty, A.T. Bell, Top. Catal. 9 (1999) 207.
[37] M.V. Frash, R.A. van Santen, J. Phys. Chem. A 104 (2000) 2468.
[38] S. Kasuriya, S. Namuangruk, P. Treesukol, M. Tirtowidjojo, J. Limtrakul, J. Catal. 219 (2003) 320.
[39] M.J. Rice, A.K. Chakraborty, A.T. Bell, J. Catal. 186 (1999) 222.
[40] J. Dedecek, D. Kaucky, B. Wichterlova, Chem. Commun. (2001) 970.
[41] N.O. Gonzales, A.K. Chakraborty, A.T. Bell, Catal. Lett. 50 (1998) 135.
[42] H.V. Koningsveld, H.V. Bekkum, J.C. Jansen, Acta Crystallogr. Sect. B Struct. Sci. B43 (1987) 127.
[43] K.-P. Schroder, J. Sauer, M. Leslie, C. Richard, A. Catlow, Zeolites 12 (1992) 20.
[44] G. Ricchiardi, J.M. Newsam, J. Phys. Chem. B 101 (1997) 9943.
[45] M.M. Francl, W.J. Pietro, W.J. Hehre, J.S. Binkley, M.S. Gordon, D.J. DeFrees, J.A. Pople, J. Chem. Phys. 77 (1982) 3654.
[46] R.C. Binning, L.A. Curtiss, J. Comput. Chem. 11 (1990) 1206.
[47] C.A. Coulson, Isr. J. Chem. 11 (1973) 683.
[48] V.A. Rassolov, M.A. Ratner, J.A. Pople, P.C. Redfern, L.A. Curtiss, J. Comput. Chem. 22 (2001) 976.
[49] A.D. Becke, J. Chem. Phys. 98 (1993) 5648.
[50] M.J. Frisch, G.W. Trucks, H.B. Schlegel, G.E. Scuseria, M.A. Robb, J.R. Cheeseman, J. Montgomery, J.A.T. Vreven, K.N. Kudin, J.C. Burant, J.M. Millam, S.S. Iyengar, J. Tomasi, V. Barone, B. Mennucci, M. Cossi, G. Scalmani, N. Rega, G.A. Petersson, H. Nakatsuji, M. Hada, M. Ehara, K. Toyota, R. Fukuda, J. Hasegawa, M. Ishida, T. Nakajima, Y. Honda, O. Kitao, H. Nakai, M. Klene, X. Li, J.E. Knox, H.P. Hratchian, J.B. Cross, C. Adamo, J. Jaramillo, R. Gomperts, R.E. Stratmann, O. Yazyev, A.J. Austin, R. Cammi, C. Pomelli, J.W. Ochterski, P.Y. Ayala, K. Morokuma, G.A. Voth, P. Salvador, J.J. Dannenberg, V.G. Zakrzewski, S. Dapprich, A.D. Daniels, M.C. Strain, O. Farkas, D.K. Malick, A.D. Rabuck, K. Raghavachari, J.B. Foresman, J.V. Ortiz, Q. Cui, A.G. Baboul, S. Clifford, J. Cioslowski, B.B. Stefanov, G. Liu, A. Liashenko, P. Piskorz, I. Komaromi, R.L. Martin, D.J. Fox, T. Keith, M.A. Al-Laham, C.Y. Peng, A. Nanayakkara, M. Challacombe, P.M.W. Gill, B. Johnson, W. Chen, M.W. Wong, C. Gonzalez, J.A. Pople, Gaussian 03, Revision B.5, Gaussian, Inc., Wallingford, CT, 2004.
[51] C.Y. Peng, H.B. Schlegel, Isr. J. Chem. 33 (1993) 449.
[52] C. Gonzalez, H.B. Schlegel, J. Chem. Phys. 90 (1989) 2154.
[53] E.R. Davidson, D. Feller, Chem. Rev. 86 (1986) 681.
[54] S.F. Boys, F. Bernardi, Mol. Phys. 19 (1970) 553.

[55] J. Dedecek, D. Kaucky, B. Wichterlova, Microporous Mesoporous Mater. 35–36 (2000) 483.
[56] A.A. Shubin, G.M. Zhidomirov, A.L. Yakovlel, R.A. van Santen, J. Phys. Chem. B 105 (2001) 4928.
[57] L.A.M.M. Barbosa, R.A. van Santen, J. Hafner, J. Am. Chem. Soc. 123 (2001) 4530.
[58] A. Bhan, Y.V. Joshi, W.N. Delgass, K.T. Thomson, J. Phys. Chem. B 107 (2003) 10476.
[59] X. Rozanska, T. Demuth, F. Hutschka, J. Hafner, R.A. van Santen, J. Phys. Chem. B 106 (2002) 3248.
[60] V. Gabova, J. Dedecek, J. Cejka, Chem. Commun. (2003) 1196.
[61] A.P. Scott, L. Radom, J. Phys. Chem. 100 (1996) 16502.